Inorganic Chemistry

Article

pubs.acs.org/IC

A DFT Study: Why Do $[Ni(P^R_2N^{R'}_2)_2]^{2+}$ Complexes Facilitate the Electrocatalytic Oxidation of Formate?

Liqin Xue and Mårten S. G. Ahlquist*

Division of Theoretical Chemistry & Biology, School of Biotechnology, KTH Royal Institute of Technology, SE-10691 Stockholm, Sweden

Supporting Information

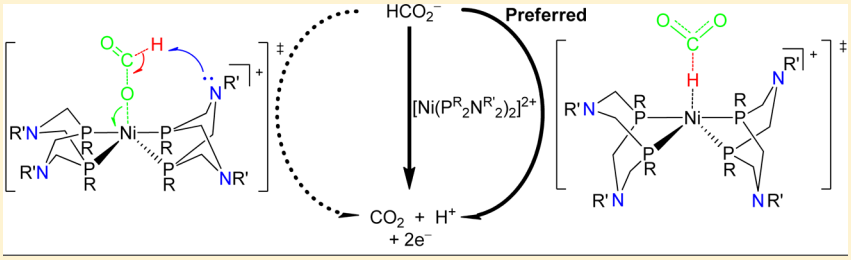

ABSTRACT: We present a DFT study of the reaction mechanism on electrocatalytic oxidation of formate by a family of $[Ni(P^R_2N^{R'}_2)_2]^{2+}$ complexes ($P^R_2N^{R'}_2$ = 1,5-diR′-3,7-diR derivative of 1,5-diaza-3,7-diphosphacyclooctane, where R and R′ are aryl or alkyl groups). $[Ni(P^{Ph}_2N^{Me}_2)_2]^{2+}$ complex **1** was used as a model complex to mimic a family of $[Ni(P^R_2N^{R'}_2)_2]^{2+}$ complexes. Our calculated results show that the decarboxylation step (corresponding to **TS3**) is the rate-determining step for the electrocatalytic oxidation of formate and that a Ni^{II}−H intermediate is involved in the reaction mechanism. The pendant amine plays an important role in the deprotonation of the nickel hydride complex generated in the decarboxylation step. In addition, our study indicates that the choice of external bases is important for removing the proton (H^+) from the nitrogen-protonated nickel(0) complexes. For the electrocatalytic oxidation of formate using the catalytically inactive $[Ni(depe)_2]^{2+}$ (depe = 1,2-bis(diethylphosphino)ethane) complex, calculations on **1-depe** have also been carried out for comparison.

INTRODUCTION

For renewable energy sources such as solar and wind to be practical, storage of the energy is crucial. H_2, as the simplest nonfossil fuel, has attracted much attention in recent years. The processes of hydrogen production in industry via the water-gas shift or methane steam re-forming require high temperatures with precious metals[1] (such as Ru, Ir, etc.) as catalysts. Since this production relies on fossil resources, the design of catalysts that can potentially be used to make hydrogen from renewable energy sources is important. Such catalysts should preferentially be based on nonprecious and abundant metals for reduction of two protons by two electrons to form H_2 (eq 1). In nature, the

$$2H^+ + 2e^- \overset{[M]}{\rightleftharpoons} H_2 \quad (1)$$

FeFe-based hydrogenases[2] and the NiFe-based hydrogenases[3] are well-known as highly efficient catalysts to produce H_2 under ambient conditions. Lately, hydrogen production from formic acid using iron catalysts, as a functional hydrogenase mimic, and its reversible process (eq 2) have been reported by Beller et al.,[4] and a theoretical investigation of the reaction mechanism for an iron-catalyzed dehydrogenation of formic acid has been reported by our group.[5] Furthermore, a family of $[Ni(P^R_2N^{R'}_2)_2]^{2+}$ complexes ($P^R_2N^{R'}_2$ = 1,5-diR′-3,7-diR derivative of 1,5-diaza-3,7-diphosphacyclooctane) with R = Ph and R′ = Ph, R = Ph and R′ = PhOMe, R = Cy and R′ = Ph, R = Cy and R′ = Bn, etc. (eq 3) as artificial hydrogenases has been also synthesized and characterized by DuBois' group.[6−8] Kubiak et al.[9] further developed the route for the synthesis of $P^R_2N^{R'}_2$ ligand with a multitude of substituents R on the phosphine.

$$HCO_2H \overset{[Fe]}{\rightleftharpoons} CO_2 + H_2 \quad (2)$$

Experimental results showed that the $[Ni(P^R_2N^{R'}_2)_2]^{2+}$ complexes, as electrocatalysts, are able to catalyze proton reduction and hydrogen oxidation (eq 1)[6] and oxygen reduction with hydrogen.[7] Theoretical studies on the proton reduction mechanism catalyzed by a $[Ni(P^H_2N^H_2)_2]^{2+}$ complex[10] and $[Ni(P^R_2N^{R'}_2)_2]^{2+}$ (R = R′ = Me, R = R′ = Ph, or R = Cy and R′ = Me) complexes[11] have been reported. Very recently, the oxidation of formate by $[Ni(P^R_2N^{R'}_2)_2]^{2+}$ complexes (eq 3) has been reported.[8] Formic acid, as one of the major products formed in biomass processing, has attracted considerable attention as a potential liquid fuel and hydrogen

Received: April 2, 2013
Published: March 18, 2014

   dx.doi.org/10.1021/ic4027317 | Inorg. Chem. 2014, 53, 3281−3289

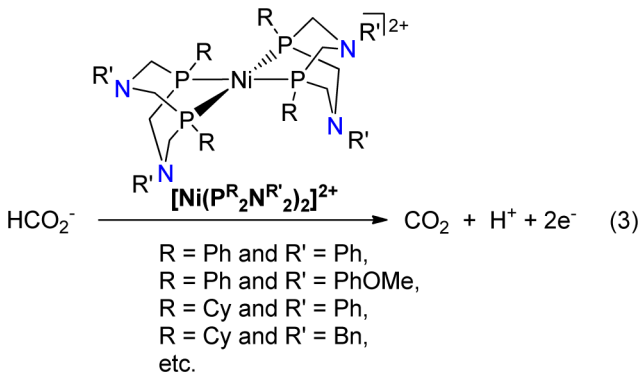

storage material.[12] The reversible process, namely converting CO_2 to formate, is of course also of interest as a method for storing hydrogen and capturing carbon dioxide.

DuBois et al.[8] proposed the reaction mechanism for formate oxidation in the original report on the basis of the following experimental results they observed. First, the TOF for the electrocatalytic formate oxidation correlating with the pK_a values of the free primary ammonium ($R'NH_3^+$) used to make the corresponding $P^R_2N^{R'}_2$ ligands follows two separate linear trend lines, where the $[Ni(P^{Ph}_2N^{R'}_2)_2]^{2+}$ complexes follow one, while the $[Ni(P^{Cy}_2N^{R'}_2)_2]^{2+}$ complexes follow another. These two linear correlations for the catalytically active $[Ni(P^R_2N^{R'}_2)_2]^{2+}$ complexes and the catalytically inactive $[Ni(depe)_2]^{2+}$ complex suggest that the rate-determining step requires the presence of the pendant amine. Second, the cyclic voltammograms for the complex $[Ni(P^{Ph}_2N^{PhOMe}_2)_2]^{2+}$ in acetonitrile solution shows that there are two reversible one-electron waves for respective Ni(II/I) and Ni(I/0) couples. The electrocatalytic formate oxidation by a $[Ni(P^{Ph}_2N^{PhOMe}_2)_2]^{2+}$ complex occurred along with the peak potential at around −0.80 V vs $Cp_2Fe^{+/0}$. Third, the peak potential for the $[NiH(P^{Ph}_2N^{PhOMe}_2)_2]^{+}$ complex was observed at −0.50 V vs $Cp_2Fe^{+/0}$. The peak potential for $[NiH(P^{Ph}_2N^{PhOMe}_2)_2]^{+}$ was not affected by addition of a stoichiometric amount of NEt_3 as an external base. On the basis of these observations the mechanism involving heterolytic cleavage of formate (i.e., β-deprotonation) was proposed by DuBois et al. as the operating mechanism in electrocatalytic formate oxidation.[8]

For the proposed mechanism as shown in Scheme 1, there are four main steps: (1) dissociation of the solvent molecule acetonitrile (ACN) from complex **A** to form complex **B**, (2) coordination of an HCO_2^- anion to complex **B** to give the five-coordinated complex **C**, (3) heterolytic cleavage of formate from complex **C** via **TS** to generate complex **D**, and (4) deprotonation from **D** and followed by oxidation to regenerate Ni^{II} complex **B** and complete the electrocatalytic cycle.[8]

Scheme 1. Proposed Mechanism for Electrocatalytic Formate Oxidation

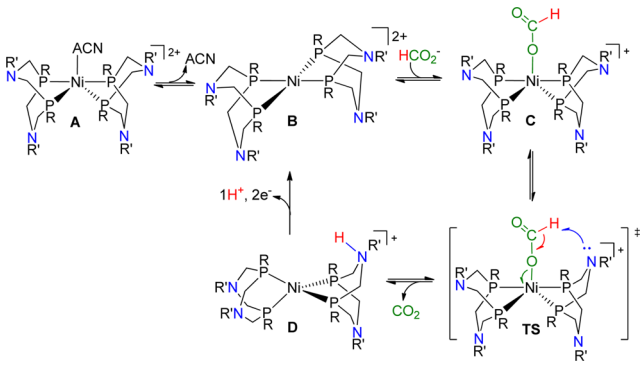

To our knowledge, no theoretical studies are available on the mechanism of catalytic electrochemical oxidation of formate in the literature. In this paper, we report our study on the reaction mechanism for the electrocatalytic formate oxidation by $[Ni(P^R_2N^{R'}_2)_2]^{2+}$ complexes reported by DuBois and co-workers[8] from a theoretical perspective. We aim to understand the details of the reaction mechanism and rationalize how $[Ni(P^R_2N^{R'}_2)_2]^{2+}$ complexes facilitate the oxidation of formate to CO_2 and the major role of pendant amine in the $[Ni(P^R_2N^{R'}_2)_2]^{2+}$ complexes for the formate oxidation reaction. Through this study, we would like to provide knowledge of development and design for these electrocatalysts for the interconversion of formate and CO_2.

COMPUTATIONAL DETAILS

All calculations were performed with the Jaguar 7.6 program package.[13] Molecular geometries of the model complexes were optimized at the Becke three-parameter hybrid functional and the LYP correlation functional (B3LYP[14]) with the LACVP** basis set,[15] while single-point energy corrections were performed with the M06[16] functional using the LACV3P**++ basis set[17] augmented with two f functions on the metal as suggested by Martin.[18] Frequency calculations at the B3LYP/LACVP** level were performed on the optimized geometries to verify that the geometries correspond to minima or first-order saddle points (transition states) on the potential energy surface (PES). All transition states were confirmed to connect to the relevant minima by intrinsic reaction coordinate (IRC)[19] calculations. On the basis of the gas-phase-optimized structures the solvation energies were estimated by single-point calculations using the Poisson−Boltzmann reactive field implemented in Jaguar 7.6 (PBF)[20] with solvent = acetonitrile, which was used under the experimental reaction conditions.[8] The estimated solvation energies were then used to correct the thermochemical data obtained from the gas-phase calculations. Since the calculations of free energy of solvation of small ionic species using the PBF method are not very reliable,[21] the solvation energies of HCO_2H, HCO_2^-, NEt_3, and Et_3NH^+ were calculated using Solvation Model 8 (SM8).[22] Hence, the Gibbs free energies were defined by the equation $G_{m06} = E_{(M06/LACV3P^{**++})} + G_{solv}$ + ZPE + H_{298} - TS_{298} + 1.9 (concentration correction to the free energy of solvation from M(g) → M(aq) to atm(g) → M(aq)). The $E_{1/2}(Fc^+/Fc)$ value is −0.624 V vs SHE (standard hydrogen electrode) in acetonitrile solution,[23] the $E_{1/2}(Ni^{II/I})$ value is −0.98 V vs $Cp_2Fe^{+/0}$ for the complex $[Ni(P^{Ph}_2N^{Me}_2)_2]^{2+}$ from experiments in acetonitrile solution,[8a] and the SHE is −4.281 V.[24] Here, we took an electron affinity of 90.5 kcal/mol (3.925 V = −0.98 V − (−0.624 V) − (−4.281 V)) to calculate the total driving force for the reaction using the $[Ni(P^{Ph}_2N^{Me}_2)_2]^{2+}$ complex. Concerning the choice of B3LYP, we also performed the calculations for Figure 2 at the B3P86[25] level as recommended in the literature.[11] The calculated results at the B3P86 level (see the Supporting Information for details) are similar to the results at B3LYP/M06 levels. In this text, we present the calculated Gibbs free energies G_{m06}, unless otherwise stated. The free energy of solvation of acetonitrile (−1.2 kcal/mol) in acetonitrile solvent was adopted from experimental results.[26]

A note should be made concerning the hydricity of the Ni−H intermediate: i.e., the thermodynamic hydride-donor ability of nickel hydride complexes (eq 4). In experiments, DuBois and co-workers investigated the hydricity by means of a thermodynamic cycle.[8] However, it is very difficult to get the absolute standard free energy of the solvated hydride ion in theoretical calculations. Here, we could

dx.doi.org/10.1021/ic4027317 | Inorg. Chem. 2014, 53, 3281−3289

$$[NiH(P^{R}{}_{2}N^{R'}{}_{2})_2]^{+} \rightleftharpoons [Ni(P^{R}{}_{2}N^{R'}{}_{2})_2]^{2+} + H^{-} \quad \Delta G^{\circ}{}_{H^{-}} \tag{4}$$

employ the isodesmic reaction scheme (as shown in eqs 5 and 6) to calculate the ΔG_{H^-} value.[27] Then we calculated $\Delta G_{H^-,calcd}([NiH(P^{Ph}{}_{2}N^{Me}{}_{2})_2]^{+})$ = 55.6 kcal/mol, which is in good agreement with experimental results (56.4 kcal/mol).[8a]

$$[Ni(P^{R}{}_{2}N^{R'}{}_{2})_2]^{2+} + HCO_2^{-} \rightleftharpoons [NiH(P^{R}{}_{2}N^{R'}{}_{2})_2]^{2+} + CO_2 \quad \Delta G^{\circ} \tag{5}$$

$$HCO_2^{-} \rightleftharpoons CO_2 + H^{-} \quad \Delta G^{\circ}{}_{H^{-},exptl} = 44.2 \text{ kcal/mol} \tag{6}$$

RESULTS AND DISCUSSION

On the basis of the previous experimental results and proposed mechanism, we carried out DFT calculations to provide insight into the details of the reaction mechanism. Here, we used the model complex $[Ni(P^{Ph}{}_{2}N^{Me}{}_{2})_2]^{2+}$ (**1**), as shown in Scheme 2,

Scheme 2. Relative Free Energies of Different Conformers of the Complex $[Ni(P^{Ph}{}_{2}N^{Me}{}_{2})_2]^{2+}$

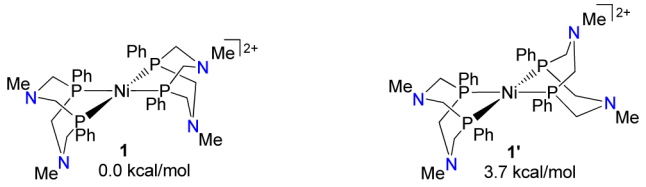

in which each diphosphine ligand contains two noncoordinating pendant amines, as the precursor complex to mimic the electrocatalysts $[Ni(P^{Ph}{}_{2}N^{R'}{}_{2})_2]^{2+}$ (R′ = PhOMe, Bn, Ph, Me). First, we considered different conformations for $[Ni(P^{R}{}_{2}N^{R'}{}_{2})_2]^{2+}$, since both boat and chair conformations for the six-membered ring were observed experimentally.[6a,8,9] DFT calculated results indicated that the lowest-energy conformers of the complexes with the $P^{Cy}{}_{2}N^{Me}{}_{2}$ and $P^{Ph}{}_{2}N^{Ph}{}_{2}$ ligands had one six-membered ring in a boat conformation and one in a chair conformation.[11b] Our calculated results (in Scheme 2) show that **1** is more stable than **1′** by 3.7 kcal/mol, which is consistent with X-ray studies, where the majority of the $[Ni(P^{R}{}_{2}N^{R'}{}_{2})_2]^{2+}$ complexes have the conformation of complex **1** in the solid state.[8]

Experimentally, complexes $[Ni(CH_3CN)(P^{R}{}_{2}N^{R'}{}_{2})_2]^{2+}$ (R = Ph and R′ = PhOMe, and R = Cy and R′ = Ph), having a fifth coordinating CH_3CN ligand, were also characterized by X-ray crystallography.[8] We optimized structures with a solvent CH_3CN molecule coordinating to complexes **1** and **1′**. Using B3LYP in the optimization resulted in dissociation of the CH_3CN ligand, however. When we performed the optimization using B3P86,[25] we could locate structures where the CH_3CN coordinated at the fifth coordination site. Using the B3P86 structure, the energy of **2** was calculated to be slightly less stable than **1** + CH_3CN by 1.7 kcal/mol (as shown in eq 7), which could indicate that **1** and **2** are in equilibrium. We do not believe that formation of **2** will have any significant impact on the reaction, since the coordinating ability of formate (HCO_2^{-})

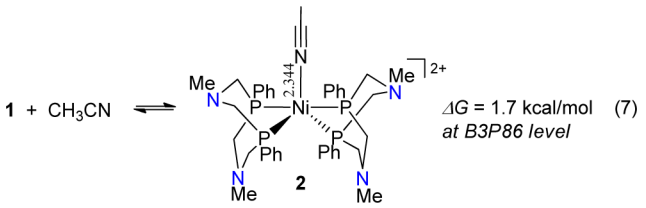

(7)

to $[Ni(P^{R}{}_{2}N^{R'}{}_{2})_2]^{2+}$ complexes is much stronger than that of CH_3CN, due to the strong electrostatic interactions between the formate anion and the $[Ni(P^{R}{}_{2}N^{R'}{}_{2})_2]^{2+}$ cation. We have therefore used complex **1** as our precursor complex in our calculations.

Direct Heterolytic Cleavage of Formate. First, we present the calculations based on the proposed mechanism: i.e., heterolytic cleavage of formate. Figure 1 shows the free

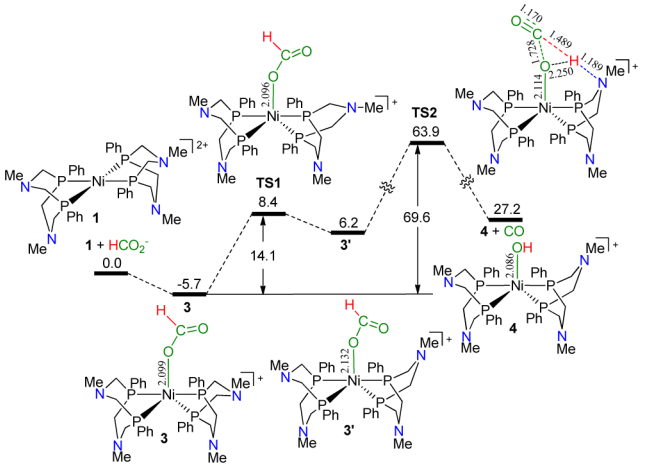

Figure 1. Energy profile calculated for the direct heterolytic cleavage of formate electrocatalyzed by complex **1**. The relative solvation-corrected Gibbs free energies are given in kcal/mol, and selected bond distances are given in Å.

energy profile for the direct heterolytic cleavage of formate electrocatalyzed by complex **1**. There are two major steps: inversion of the pendant amine and heterolytic cleavage of formate. A formate anion (HCO_2^{-}) first coordinates to complex **1** to form the five-coordinate complex **3**. Followed by inversion of one of pendant amines from the chair to the boat conformation in complex **3** via **TS1**, complex **3′** is formed, which is set up for the heterolytic cleavage of formate. Then complex **3′** undergoes cleavage of formate (**TS2**), which a bit surprisingly leads to the formation of the nickel hydroxy complex **4** and CO. In **TS2** the H atom of the formate ligand reacts with the lone pair of the N atom in the pendant amine. The scan of the intrinsic reaction coordinate (IRC) for **TS2** showed that the reaction gives CO instead of CO_2 as product, which is very different from the proposed mechanism: i.e., heterolytic cleavage with CO_2 as the product. Despite several attempts (we have tried controlling the N−H distances, the C−H distances, or both N−H and C−H distances), we have not been able to find any transition state of a direct heterolytic cleavage for formate connecting complex **3** and the nitrogen-protonated nickel(0) complex **D** with CO_2. Following **TS2** the proton first resides on the nitrogen and then spontaneously moves over to the oxygen on the nickel center.

dx.doi.org/10.1021/ic4027317 | Inorg. Chem. 2014, 53, 3281−3289

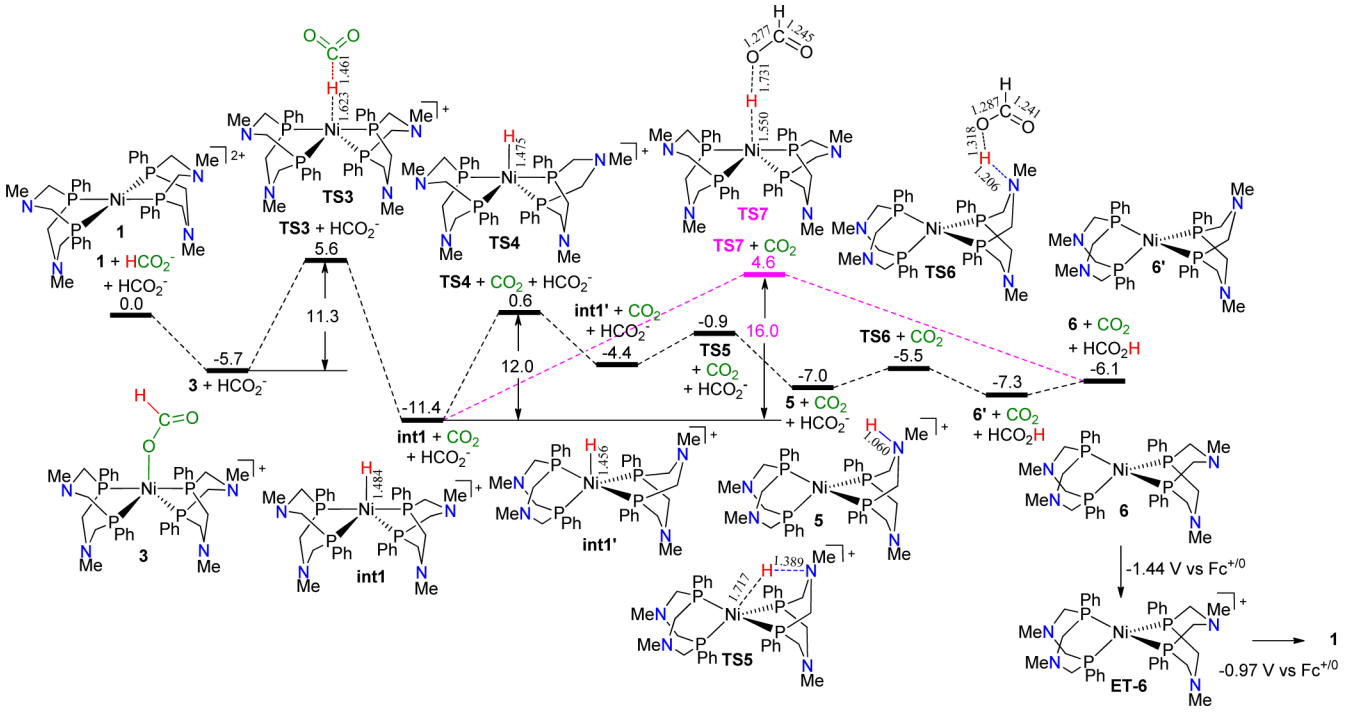

Figure 2. Energy profiles calculated for the direct hydride transfer mechanism of electrocatalytic oxidation of formate by $[Ni(P^{Ph}_2N^{Me}_2)_2]^{2+}$ complex **1**. The relative solvation-corrected Gibbs free energies are given in kcal/mol, and selected bond distances are given in Å. The favorable pathway is shown by a black dashed line, and another possible pathway for the direct deprotonation is shown by a pink dashed line.

Our results show that the direct heterolytic cleavage of formate is an endergonic process with an energy of 27.2 kcal/mol. The overall barrier (corresponding to **TS2**) for the heterolytic cleavage of formate is 69.6 kcal/mol. The inversion (corresponding to **TS1**) step from **3** to **3**′ is relatively facile. Our calculated results suggest that the proposed mechanism by DuBois et al. for formate oxidation via the direct heterolytic cleavage of formate process is unlikely.

Direct Hydride Transfer Mechanism of Electrocatalytic Oxidation of Formate via a Ni^{II}–H Intermediate. Next we discuss another possible mechanism for the formate oxidation. Both β-hydride elimination and direct hydride transfer are well-known mechanisms for hydride transfers to metal centers. In the current case β-hydride elimination is unlikely, since it requires a vacant cis coordination site. Therefore, we tested an alternative mechanism, a direct hydride transfer from formate to the metal via a Ni^{II}–H intermediate.

Figure 2 depicts energy profiles of calculated relative solvation-corrected Gibbs free energies for electrocatalytic oxidation of formate. For the favorable pathway as shown in black in Figure 2, the overall reaction of formate oxidation consists of five main steps: (1) **1** + HCO_2^- → **int1** coordination of HCO_2^- to give **3** followed by decarboxylation via **TS3** with a barrier of 11.3 kcal/mol relative to complex **3** to give the Ni^{II}–H intermediate **int1** and release CO_2, (2) **int1** → **int1**′ inversion of one of the six-membered rings from the chair conformation to the boat conformation via **TS4** with a barrier of 12.0 kcal/mol relative to the intermediate **int1** to form the intermediate **int1**′, (3) **int1**′ → **5** internal proton transfer from the Ni^{II}–H intermediate **int1**′ to give the nitrogen-protonated nickel(0) complex **5** via **TS5** with a barrier of 10.5 kcal/mol relative to intermediate **int1**, (4) **5** → **6** deprotonation via **TS6** followed by inversion giving the nickel(0) complex **6**, (5) **6** → **1** reoxidation via **ET-6** to complete the electrocatalytic cycle and regenerate the precursor complex **1**.

The overall reaction $2HCO_2^- \rightarrow CO_2 + HCO_2H + 2e^-$ is an exergonic process with a reaction energy of −16.5 kcal/mol. The highest solvation-corrected Gibbs free energy barrier for a formate oxidation process catalyzed by precursor complex **1** was calculated to be 12.0 kcal/mol, corresponding to **TS4** relative to **int1**. Furthermore, the barrier for decarboxylation (**TS3**) is 11.3 kcal/mol, which is competitive with **TS4**. Therefore, both **TS3** and **TS4** have the possibility to be the rate-determining step. The R′ substituent (R′ = aryl group) on the N atom in the $[Ni(P^R_2N^{R'}_2)_2]^{2+}$ complexes will decrease the barrier energy of **TS4**, since the lone pair of the electron on N atom in ligands of $P^R_2N^{R'}_2$ can be conjugated to the π system of the aryl ring, which can stabilize transition state **TS4**. Furthermore, the electronic energies relative to the preceding intermediates (ΔE) are 17.7 kcal/mol for **TS3** and 11.7 kcal/mol for **TS4**. It is possible that some of the corrections that are made to the free energy are erroneous, leading to the free energy of **TS3** (11.3 kcal/mol) being underestimated. The conformational change in **TS4** gives a small error in free energy correction. Therefore, we believe that the decarboxylation step (**TS3**) is the rate-determining step in the whole electrocatalytic formate oxidation reaction.

In order to understand the role of the pendant amine, we also calculated a direct deprotonation step from **int1** to **6**. As shown in pink in Figure 2, the barrier (corresponding to **TS7**) for direct deprotonation is 16.0 kcal/mol, which is significantly higher than the barrier of the process with the pendant amine assistance pathway (i.e., the process goes through **TS5** and **TS6** with a barrier of 10.5 kcal/mol) and would be the rate-determining step if the amine were not present. Hence, the pendant amine plays an important role in the electrocatalytic

dx.doi.org/10.1021/ic4027317 | Inorg. Chem. 2014, 53, 3281−3289

formate oxidation by $[Ni(P^{R}_{2}N^{R'}_{2})_2]^{2+}$ complexes. The direct hydride transfer mechanism via a Ni^{II}–H intermediate followed by deprotonation with assistance of the pendant amine appears likely.

As suggested by one reviewer, we performed further calculations using the $[Ni(P^{Ph}_{2}N^{Ph}_{2})_2]^{2+}$ complex. As shown in Figure 3, the $[Ni(P^{Ph}_{2}N^{Ph}_{2})_2]^{2+}$ complex $\mathbf{N^{Ph}}$**-1** was used as a

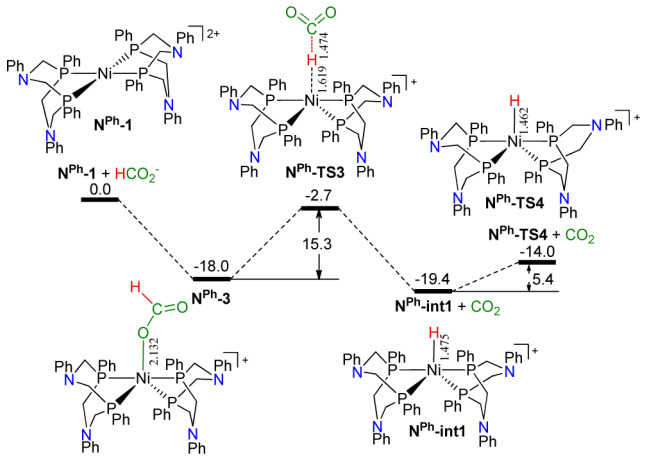

Figure 3. Energy profile calculated for decarboxylation and inversion steps by the $[Ni(P^{Ph}_{2}N^{Ph}_{2})_2]^{2+}$ complex $\mathbf{N^{Ph}}$**-1**. The relative solvation-corrected Gibbs free energies are given in kcal/mol, and selected bond distances are given in Å.

precursor complex to calculate decarboxylation and inversion steps. Formate coordinates to $\mathbf{N^{Ph}}$**-1** to form the stable species $\mathbf{N^{Ph}}$**-3**. Then the decarboxylation occurs via $\mathbf{N^{Ph}}$**-TS3** with a free energy barrier of 15.3 kcal/mol relative to $\mathbf{N^{Ph}}$**-3** to generate $\mathbf{N^{Ph}}$**-int1**. Since the hydride transfer needs the assistance of the pendant amine, the inversion via $\mathbf{N^{Ph}}$**-TS4** will occur to put the N atom in the pendant amine close to the hydride H atom. The barrier of $\mathbf{N^{Ph}}$**-TS4** is 5.4 kcal/mol, which is much lower than that of $\mathbf{N^{Ph}}$**-TS3**, as expected. Clearly, the decarboxylation step is the rate-determining step with an activation energy of 15.3 kcal/mol, which is consistent with the experimental value (16.0 ± 1.7 kcal/mol).

Understanding the Role of Pendant Amine in Complexes $[Ni(P^{R}_{2}N^{R'}_{2})_2]^{2+}$ and Barriers of TS3/TS3-depe. The calculated results show that the pendant amine in complex **1** plays a very important role in the deprotonation step. In experiments, $[Ni(depe)_2]^{2+}$ shows very low catalytic activity for formate oxidation.[8a] To compare the formate oxidation capability of the $[Ni(depe)_2]^{2+}$ complex **1-depe** with that of complex **1**, we also calculated the possible intermediates via decarboxylation followed by deprotonation of the Ni^{II}–H intermediate with depe ligands. Figure 4 shows the solvation-corrected Gibbs free energy profile calculated for the formate oxidation by the $[Ni(depe)_2]^{2+}$ complex **1-depe**. After formation of **3-depe** by coordination of a formate anion to **1-depe**, the decarboxylation occurs via **TS3-depe** with a barrier of 18.8 kcal/mol relative to **3-depe**. Since there is no pendant amine in the depe ligand, only the direct deprotonation of the resulting intermediate **int1-depe** could occur via **TS7-depe** with the barrier of 20.4 kcal/mol to give the nickel(0) complex **6-depe**. The difference in activation free energy for the steps involving **TS3-depe** and **TS7-depe** is only 1.6 kcal/mol. Since the difference is quite small, we only could conclude that these

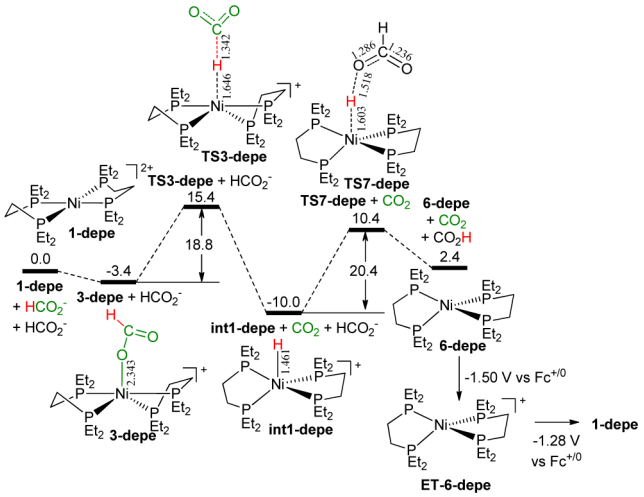

Figure 4. Energy profile calculated for the formate oxidation by the $[Ni(depe)_2]^{2+}$ complex **1-depe**. The relative solvation-corrected Gibbs free energies are given in kcal/mol, and selected bond distances are given in Å.

two steps are competitive and either of them could be the rate-determining step.

Concerning the nature of **TS3**/**TS3-depe** and **TS7**/**TS7-depe** in a solvent medium, we also carried out calculations for **TS3**/**TS3-depe** and **TS7**/**TS7-depe** with a solvation model. We located all these transition states in solution, which showed structures similar to those optimized under vacuum (see the Supporting Information for details).

From the above results, we can see that the pendant amine in the ligand of $P^{R}_{2}N^{R'}_{2}$ plays an important role not only in the deprotonation step but also in the decarboxylation step. In the deprotonation the role of the amine is clearer, since it is directly involved, but in the decarboxylation the role seem to be an indirect one, where it modulates the properties of the nickel center. In the following part we attempt to analyze the difference between these two different types of ligands, namely, the ligand of $P^{R}_{2}N^{R'}_{2}$ with pendant amines and the ligand of depe without pendant amine.

In the whole process, the formation of Ni^{II}–H intermediates **int1**/**int1-depe** is one of the crucial steps. Therefore, we want to investigate the difference between barriers **TS3**/**TS3-depe**. The activation strain model is a fragment-based approach to analyze the activation energies, where the activation energy ΔE is decomposed into the strain ΔE_{strain} of the deformed reactants and the interaction ΔE_{int} between these deformed reactants: i.e., $\Delta E = \Delta E_{strain} + \Delta E_{int}$. Since the CO_2 and nickel hydride intermediate are generated after decarboxylation (via **TS3**/**TS3-depe**), and the reverse reaction follows the same trend in reactivity among these complexes, we carried out an activation strain analysis[28] for **TS3**/**TS3-depe** of the respective reverse reactions (**int1**/**int1-depe** → **3**/**3-depe**) barriers in order to analyze the difference between using $[Ni(P^{R}_{2}N^{R'}_{2})_2]^{2+}$ with catalytic activity and $Ni[(depe)_2]^{2+}$ with low catalytic activity. It is worth mentioning that the transition states (**TS3**/**TS3-depe**) are a route of transferring an electron pair from the nickel–hydride bond to the incoming CO_2, and this electron pair goes into an antibonding π orbital to form a carboxylate anion, which is naturally bent.

As shown in Scheme 3, the strain of the nickel hydride complex and carbon dioxide leads to destabilization of the

dx.doi.org/10.1021/ic4027317 | Inorg. Chem. 2014, 53, 3281–3289

Scheme 3. Activation Strain Analysis for TS3/TS3-depe

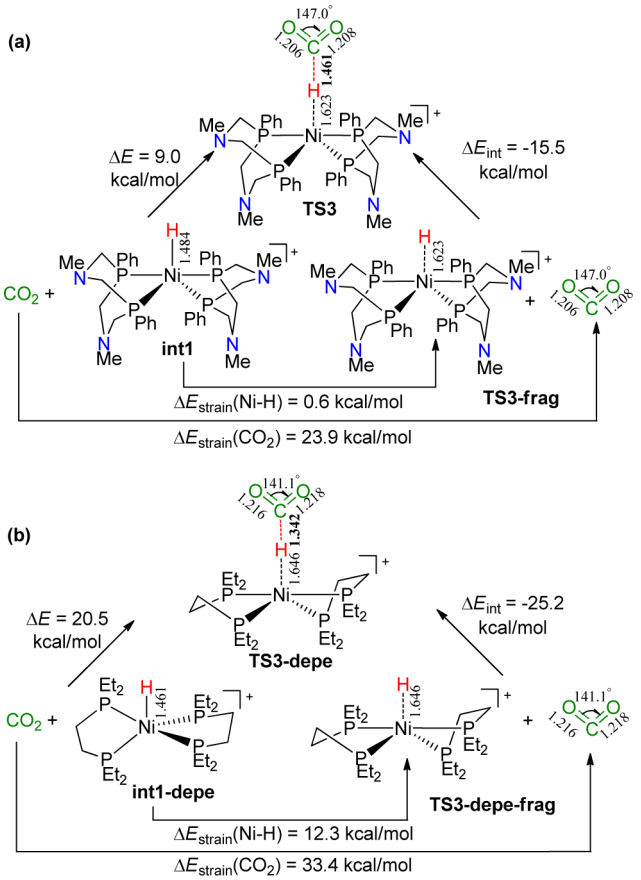

transition state, while the interaction of the deformed carbon dioxides with the deformed nickel hydride complex leads to stabilization of the transition state. Scheme 3a shows calculated results for **TS3** that ΔE_{strain} values of the Ni−H complex **int1** and CO_2 are 0.6 and 23.9 kcal/mol, respectively, and the ΔE_{int} value between the deformed Ni−H and CO_2 is −15.5 kcal/mol. Clearly, the main energy cost at transition state **TS3** is the strain of CO_2. The calculated strain analysis results for **TS3-depe** are shown in Scheme 3b. The strains of **int1-depe** and CO_2 are 12.3 and 33.4 kcal/mol, respectively, and the interaction energy is −25.2 kcal/mol. This shows that **TS3-depe** involves more strain of both **int1-depe** and CO_2 than **TS3** does. The main difference between these two types of complexes $[Ni(P^{Ph}{}_2N^{Me}{}_2)_2]^{2+}$ and $Ni[(depe)_2]^{2+}$ is the energy costs in strain of **int1** and **int1-depe**. Examining and comparing the structures of **int1**, **TS3**, **int1-depe**, and **TS3-depe**, we find that the Ni−H distance in **TS3** (1.623 Å) is shorter than that in **TS3-depe** (1.646 Å), and the C−H distance in **TS3** (1.461 Å) is longer than that in **TS3-depe** (1.342 Å). To summarize this part, it appears that the more the transition state resembles the Ni−H intermediate and carbon dioxide, the lower the barrier is, for both the forward and reverse reactions.

Analysis of the molecular orbitals of **int1** and **int1-depe** (as shown in Figure 5) shows that the filled Ni−H σ orbital HOMO of **int1** (−0.206638 au) is higher in energy than HOMO-2 of **int1-depe** (−0.245960 au), supporting the notion that **int1** is a better nucleophile to react with CO_2. Furthermore, the energy for the LUMO of **int1** (−0.051861 au) is lower than that of **int1-depe** (−0.036535 au), suggesting that hydride in **int1** is also a better electrophile to accept the

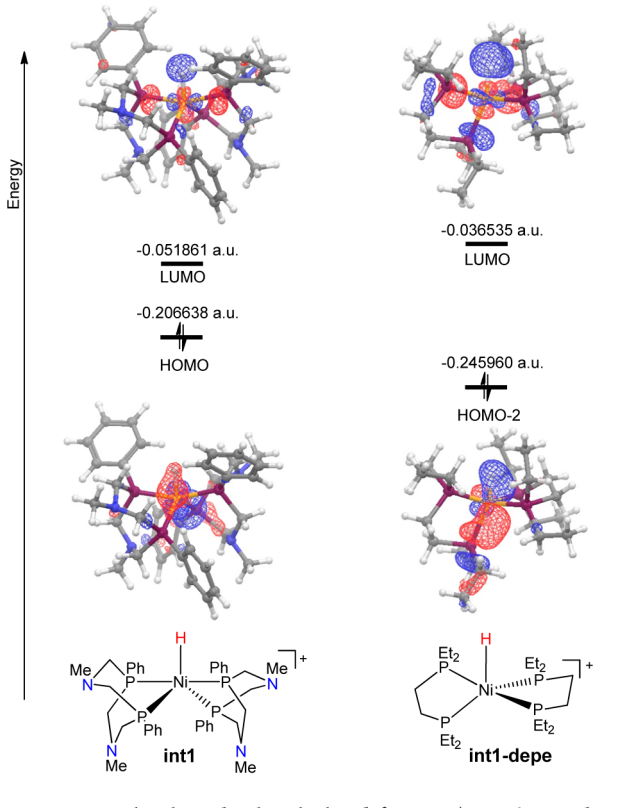

Figure 5. Molecular orbitals calculated for **int1**/**int1-depe**. The orbital energies are given in atomic units (au).

electron pair from either the formate anion or the pendant amine in the ligand, which explains why the energy of the barrier **TS7** is lower than that of **TS7-depe**.

Comparison between Theoretical Results and Experimental Observations. *(a). Oxidation of Ni^{II}−H Intermediate.* As we mentioned in the Introduction, the peak potential for $[NiH(P^{Ph}{}_2N^{PhOMe}{}_2)_2]^+$ was observed at −0.50 V vs $Cp_2Fe^{+/0}$ in experiments. We calculated the redox potential for $[NiH(P^{Ph}{}_2N^{Me}{}_2)_2]^+$ in order to understand the experimental results. Here, we use **ET** to label the complexes or intermediates resulting from one-electron transfer (ET). As shown in Scheme 4, the calculated potential is −0.64 V (0.14 V

Scheme 4. Calculated Redox Potential for int1

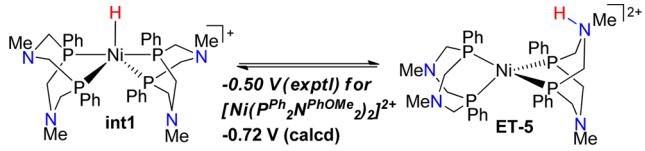

negative shift) for the Ni^{II}−H couple: namely, **int1**/**ET-5**. This negative shift is caused by the model complex using a Me substituent on N atoms in the ligands.

(b). Ni^{II}−H Intermediate in the Presence of NEt_3 as an External Base. With the presence of a stoichiometric amount of NEt_3, the peak potential for $[NiH(P^{Ph}{}_2N^{PhOMe}{}_2)_2]^+$ was not changed,[8b] suggesting that there is no reaction between $[NiH(P^{Ph}{}_2N^{PhOMe}{}_2)_2]^+$ and NEt_3. Figure 6 illustrates the free energy profiles for the deprotonation processes with or without assistance by the pendant amine.

dx.doi.org/10.1021/ic4027317 | Inorg. Chem. 2014, 53, 3281−3289

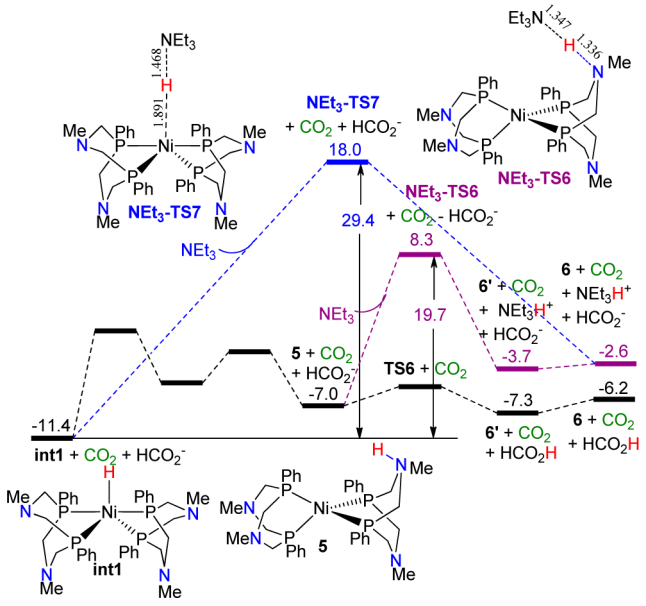

Figure 6. Energy profiles calculated for the deprotonation processes with the external base NEt_3. The schematic results in black use an HCO_2^- anion as the external base. The deprotonation process with assistance by the pendant amine is shown in purple, and the direct deprotonation process is shown in blue.

As shown in purple, the energy barrier of **NEt$_3$-TS6** (19.7 kcal/mol) is much higher than that of **TS6** (5.9 kcal/mol), where the external base is a formate anion. For direct deprotonation from the Ni^{II}–H complex **int1**, shown in blue, the energy barrier of **NEt$_3$-TS7** is 29.4 kcal/mol. Both deprotonation processes using NEt_3 as an external base show barriers higher than those using HCO_2^- as the base and are significantly more endergonic. These results suggest that the external base also plays an important role in the overall formate oxidation reaction, especially in the deprotonation step. If the base cannot deprotonate either the Ni^{II}–H intermediate **int1** or the nitrogen-protonated nickel(0) intermediate **5**, the reaction will be stopped by the deprotonation step, namely, **int1** followed by oxidation to give **ET-5**, which could explain the observation that the peak potential for $[NiH(P^R_2N^{R'}_2)_2]^+$ complexes is around −0.50 V vs $Cp_2Fe^{+/0}$ in experiments, with or without NEt_3. On the basis of these results we suggest an experiment where the added base is a carboxylate, since carboxylate bases are more basic than alkylamines in acetonitrile.

(c). Reaction Using $[Ni(P^{Ph}_2N^{PhOMe}_2)_2]^{2+}$ Complex with the Presence of HCO_2^- as an External Base. In experiments, the electrocatalytic formate oxidation by $[Ni(P^{Ph}_2N^{PhOMe}_2)_2]^{2+}$ occurred along with the peak potential at around −0.80 V vs $Cp_2Fe^{+/0}$.[8b] As we discussed above, the whole process for the formate oxidation using formate as an external base is facile. First, **int1** will undergo deprotonation with the assistance of a pendant amine and the external base HCO_2^- to remove the proton from **int1** and give the Ni(0) complex $[Ni(P^{Ph}_2N^{Me}_2)_2]$ (**6**). Second, the Ni(0) complex **6** will be easily oxidized to the Ni(I) complex **ET-6**. In other words, the process involves a proton transfer to an external base, which is likely to affect the reduction potential. The stronger base facilitates deprotonation, giving sufficient concentration of Ni(0) for oxidation to be observed.

In experiments, the Ni(I/0) couple vs $Cp_2Fe^{+/0}$ still can be observed in the presence of HCO_2^-.[8b] The calculated Ni(I/0) couple is −1.44 V vs $Cp_2Fe^{+/0}$, which has a −0.30 V shift in comparison with the experimental value of −1.14 V vs $Cp_2Fe^{+/0}$.[8a]

Correlation between TOF and pK_a vs Correlation between TOF and Ni Redox Potential. In the original report, DuBois et al. plotted the TOF for electrocatalytic formate oxidation vs the pK_a of the free primary ammonium ($R'NH_3^+$) used to synthesize the $P^R_2N^{R'}_2$ ligands in each nickel(II) complex.[8] There are two separate trend lines observed in their plot, with $[Ni(P^{Ph}_2N^{R'}_2)_2]^{2+}$ complexes following one line and $[Ni(P^{Cy}_2N^{R'}_2)_2]^{2+}$ complexes following the other line. Since the basicity of nitrogen correlated with the catalytic activity, the authors concluded that the pendant amine must be directly involved in the rate-determining step.

However, on the basis of our calculated results, the decarboxylation step could be the rate-determining step in the formate oxidation reaction. Therefore, using the experimental results by DuBois et al., we plotted the TOF for electrocatalytic formate oxidation vs the $Ni^{II/I}$ potentials of $[Ni(P^R_2N^{R'}_2)_2]^{2+}$ complexes, as shown in the trend line in Figure 7, and we found that there is also an excellent

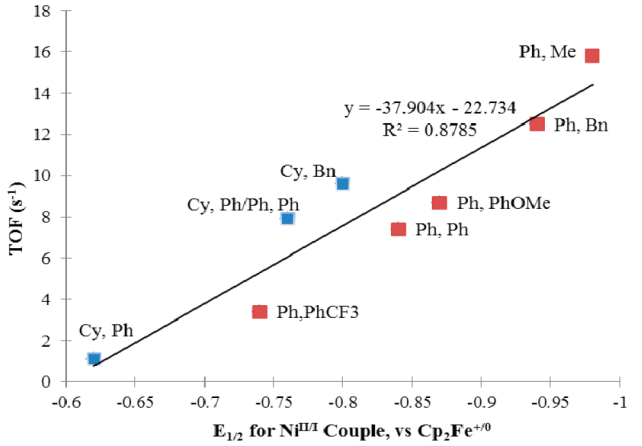

Figure 7. Correlations of TOF for the electrocatalytic formate oxidation with $Ni^{II/I}$ reduction potentials. Experimental data are adapted from ref 8. The trend line shows the correlation of TOF for the electrocatalytic formate oxidation with both $[Ni(P^{Cy}_2N^{R'}_2)_2]^{2+}$ (in blue) and $[Ni(P^{Ph}_2N^{R'}_2)_2]^{2+}$ (in red).

correlation. This correlation suggests that the different substituents R and R′ on P and N atoms, respectively, will affect the reduction potentials of $[Ni(P^R_2N^{R'}_2)_2]^{2+}$ complexes and could affect the TOF of electrocatalytic formate oxidation by modulating the electronic properties of $[Ni(P^R_2N^{R'}_2)_2]^{2+}$ complexes.

CONCLUSION

In this paper we have reported a theoretical study on the reaction mechanism of the electrocatalytic oxidation of formate by $[Ni(P^{Ph}_2N^{Me}_2)_2]^{2+}$ (**1**).

For the previously proposed heterolytic cleavage of formate mechanism, the activation free energy (corresponding to **TS2**) was calculated to be extremely high (69.6 kcal/mol). Moreover,

dx.doi.org/10.1021/ic4027317 | Inorg. Chem. 2014, 53, 3281−3289

an intrinsic reaction coordinate of **TS2** calculations showed that CO is generated during this heterolytic cleavage process, which excludes the heterolytic cleavage mechanism for formate oxidation by a family of $[Ni(P^{R}_{2}N^{R'}_{2})_{2}]^{2+}$ complexes.

Instead, we find that the direct hydride transfer mechanism for formate oxidation is a plausible reaction mechanism. Our results show that the formate-coordinated complex **3** undergoes a direct hydride transfer (via **TS3**) to eject CO_2 and form the Ni^{II}–H intermediate **int1**. Then **int1** can undergo an inversion step to give **int1′** followed by an internal proton transfer to give **5**. The external base HCO_2^- abstracts the proton from **5** to form **6′**; following an inversion, **6** will be formed. Finally reoxidation of **6** via **ET-6** gives complex **1** to complete the electrocatalytic cycle.

For the direct hydride transfer mechanism, the decarboxylation step (**TS3**/$\mathbf{N^{Ph}}$**-TS3**) is the rate-determining step in the whole reaction. The pendant amine in $[Ni(P^{R}_{2}N^{R'}_{2})_{2}]^{2+}$ complexes plays an very important role in the internal proton transfer step. A comparison of the formate oxidation reaction using catalytically inactive $[Ni(depe)_2]^{2+}$ complex **1-depe** shows that the function of the pendant amine is not only to assist the proton transfer from the nickel metal center to the external base but also to modulate the properties of the Ni^{II} metal center so that all the steps are facile. In addition the choice of external base is important for the oxidation of the Ni^{II}–H intermediate to Ni^{II} (via Ni^0) and a proton.

Finally, the results of activation strain analysis of the reaction barriers (**TS3**/**TS3-depe**) suggest that the design of new catalysts with a small strain of the catalysts could be promising for improved catalytic conversion between formate and CO_2.

■ ASSOCIATED CONTENT

Supporting Information

Text, figures, and tables giving additional data and all of the energy components and Cartesian coordinates for all of the calculated structures. This material is available free of charge via the Internet at http://pubs.acs.org.

■ AUTHOR INFORMATION

Corresponding Author

*E-mail for M.S.G.A.: mahlquist@theochem.kth.se.

Notes

The authors declare no competing financial interest.

■ ACKNOWLEDGMENTS

The authors acknowledge financial support from the Vetenskapsrådet. We thank the PDC center and the National Supercomputer Centre in Sweden (NSC) for high-performance computing.

■ REFERENCES

(1) (a) Enthaler, S.; von Langermann, J.; Schmidt, T. *Energy Environ. Sci.* **2010**, *3*, 1207 and references therein. (b) Federsel, R.; Jackstell, A.; Boddien, G.; Laurenczy; Beller, M. *ChemSusChem* **2010**, *3*, 1048.

(2) Peters, J. W.; Lanzilotta, W. N.; Lemon, B. J.; Seefeldt, L. C. *Science* **1998**, *282*, 1853.

(3) Volbeda, A.; Charon, M. H.; Piras, C.; Hatchikian, E. C.; Frey, M.; Fontecilla-Camps, J. C. *Nature* **1995**, *373*, 580.

(4) (a) Boddien, A.; Loges, B.; Gartner, F.; Torborg, C.; Fumino, K.; Junge, H.; Ludwig, R.; Beller, M. *J. Am. Chem. Soc.* **2010**, *132*, 6480. (b) Federsel, C.; Boddien, A.; Jackstell, R.; Jennerjahn, R.; Dyson, P. J.; Scopelliti, R.; Laurenczy, G.; Beller, M. *Angew. Chem., Int. Ed.* **2010**, *49*, 9777. (c) Boddien, A.; Mellmann, D.; Gartner, F.; Jackstell, R.; Junge, H.; Dyson, P. J.; Laurenczy, G.; Ludwig, R.; Beller, M. *Science* **2011**, *333*, 1733.

(5) Sanchez-de-Armas, R.; Xue, L.; Ahlquist, M. S. *Chem. Eur. J.* **2013**, *19*, 11869.

(6) (a) Wilson, A. D.; Newell, R. H.; McNevin, M. J.; Muckerman, J. T.; Rakowski DuBois, M.; DuBois, D. L. *J. Am. Chem. Soc.* **2006**, *128*, 358. (b) Rakowski DuBois, M.; DuBois, D. L. *Chem. Soc. Rev.* **2009**, *38*, 62. (c) Rakowski DuBois, M.; Dubois, D. L. *Acc. Chem. Res.* **2009**, *42*, 1974. (d) Kilgore, U. J.; Roberts, J. A.; Pool, D. H.; Appel, A. M.; Stewart, M. P.; Rakowski DuBois, M.; Dougherty, W. G.; Kassel, W. S.; Bullock, R. M.; DuBois, D. L. *J. Am. Chem. Soc.* **2011**, *133*, 5861. (e) O'Hagan, M.; Shaw, W. J.; Raugei, S.; Chen, S.; Yang, J. Y.; Kilgore, U. J.; DuBois, D. L.; Bullock, R. M. *J. Am. Chem. Soc.* **2011**, *133*, 14301. (f) Wiedner, E. S.; Yang, J. Y.; Chen, S.; Raugei, S.; Dougherty, W. G.; Kassel, W. S.; Helm, M. L.; Bullock, R. M.; Rakowski DuBois, M.; DuBois, D. L. *Organometallics* **2012**, *31*, 144. (g) Smith, S. E.; Yang, J. Y.; DuBois, D. L.; Bullock, R. M. *Angew. Chem., Int. Ed.* **2012**, *51*, 3152. (h) Wiese, S.; Kilgore, U. J.; DuBois, D. L.; Bullock, R. M. *ACS Catalysis* **2012**, *2*, 720. (i) O'Hagan, M.; Ho, M. H.; Yang, J. Y.; Appel, A. M.; Rakowski DuBois, M.; Raugei, S.; Shaw, W. J.; Dubois, D. L.; Bullock, R. M. *J. Am. Chem. Soc.* **2012**, *134*, 19409.

(7) Yang, J. Y.; Bullock, R. M.; Dougherty, W. G.; Kassel, W. S.; Twamley, B.; DuBois, D. L.; Rakowski DuBois, M. *Dalton Trans.* **2010**, *39*, 3001.

(8) (a) Galan, B. R.; Schoffel, J.; Linehan, J. C.; Seu, C.; Appel, A. M.; Roberts, J. A.; Helm, M. L.; Kilgore, U. J.; Yang, J. Y.; DuBois, D. L.; Kubiak, C. P. *J. Am. Chem. Soc.* **2011**, *133*, 12767. (b) Seu, C. S.; Appel, A. M.; Doud, M. D.; DuBois, D. L.; Kubiak, C. P. *Energy Environ. Sci.* **2012**, *5*, 6480.

(9) Doud, M. D.; Grice, K. A.; Lilio, A. M.; Seu, C. S.; Kubiak, C. P. *Organometallics* **2012**, *31*, 779.

(10) (a) Kachmar, A.; Vetere, V.; Maldivi, P.; Franco, A. A. *J. Phys. Chem. A* **2010**, *114*, 11861. (b) Dupuis, M.; Chen, S.; Raugei, S.; DuBois, D. L.; Bullock, R. M. *J. Phys. Chem. A* **2011**, *115*, 4861.

(11) (a) Chen, S.; Raugei, S.; Rousseau, R.; Dupuis, M.; Bullock, R. M. *J. Phys. Chem. A* **2010**, *114*, 12716. (b) Raugei, S.; Chen, S.; Ho, M. H.; Ginovska-Pangovska, B.; Rousseau, R. J.; Dupuis, M.; DuBois, D. L.; Bullock, R. M. *Chem. Eur. J.* **2012**, *18*, 6493.

(12) (a) Enthaler, S. *ChemSusChem* **2008**, *1*, 801. (b) Joó, F. *ChemSusChem* **2008**, *1*, 805. (c) Grasemann, M.; Laurenczy, G. *Energy Environ. Sci.* **2012**, *5*, 8171.

(13) *Jaguar, version 7.6*; Schrödinger, LLC, New York, 2009.

(14) (a) Becke, A. D. *Phys. Rev. A* **1988**, *38*, 3098. (b) Lee, C.; Yang, W.; Parr, R. G. *Phys. Rev. B* **1988**, *37*, 785. (c) Implemented as described in: Miehlich, B.; Savin, A.; Stoll, H.; Preuss, H. *Chem. Phys. Lett.* **1989**, *157*, 200.

(15) LACVP basis sets use 6-31G for the main-group elements and the Hay–Wadt ECP for nickel: Hay, P. J.; Wadt, W. R. *J. Chem. Phys.* **1985**, *82*, 299.

(16) Zhao, Y.; Truhlar, D. G. *Theor. Chem. Acc.* **2008**, *120*, 215.

(17) The LACV3P basis set is a triple-ζ contraction of the LACVP basis set developed and tested at Schrödinger, Inc.

(18) Martin, J. M. L.; Sundermann, A. *J. Chem. Phys.* **2001**, *114*, 3408.

(19) (a) Gonzalez, C.; Schlegel, H. B. *J. Chem. Phys.* **1989**, *90*, 2154. (b) Gonzalez, C.; Schlegel, H. B. *J. Chem. Phys.* **1990**, *94*, 5523.

(20) (a) Tannor, D. J.; Marten, B.; Murphy, R.; Friesner, R. A.; Sitkoff, D.; Nicholls, A.; Ringnalda, M.; Goddard, W. A., III; Honig, B. *J. Am. Chem. Soc.* **1994**, *116*, 11875. (b) Marten, B.; Kim, K.; Cortis, C.; Friesner, R. A.; Murphy, R. B.; Ringnalda, M. N.; Sitkoff, D.; Honig, B. *J. Phys. Chem.* **1996**, *100*, 11775.

(21) Ahlquist, M.; Kozuch, S.; Shaik, S.; Tanner, D.; Norrby, P.-O. *Organometallics* **2006**, *25*, 45.

(22) Marenich, A. V.; Olson, R. M.; Kelly, C. P.; Cramer, C. J.; Truhlar, D. G. *J. Chem. Theory Comput.* **2007**, *3*, 2011.

(23) Pavlishchuk, V. V.; Addison, A. W. *Inorg. Chim. Acta* **1999**, *298*, 97.

(24) Isse, A. A.; Gennaro, A. *J. Phys. Chem. B* **2010**, *114*, 7894.

(25) (a) Becke, A. D. *Phys. Rev. A* **1988**, *38*, 3098. (b) Perdew, J. P. *Phys. Rev. B* **1986**, *33*, 8822; **1986**, *34*, 7406 (erratum).
(26) Kelly, C. P.; Cramer, C. J.; Truhlar, D. G. *J. Phys. Chem. B* **2007**, *111*, 408.
(27) (a) Muckerman, J. T.; Achord, P.; Creutz, C.; Polyansky, D. E.; Fujita, E. *Proc. Natl. Acad. Sci. U.S.A.* **2012**, *109*, 15657. (b) Curtis, C. J.; Miedaner, A.; Ellis, W. W.; DuBois, D. L. *J. Am. Chem. Soc.* **2002**, *124*, 1918. (c) Miller, A. J.; Labinger, J. A.; Bercaw, J. E. *Organometallics* **2011**, *30*, 4308.
(28) (a) Ess, D. H.; Houk, K. N. *J. Am. Chem. Soc.* **2008**, *130*, 10187. (b) van Zeist, W.-J.; Bickelhaupt, F. M. *Org. Biomol. Chem.* **2010**, *8*, 3118.

dx.doi.org/10.1021/ic4027317 | *Inorg. Chem.* 2014, 53, 3281−3289